Paper No.
13299

NACE INTERNATIONAL CORROSION Conference & Expo 2019

Corrosion, Scaling and Material Selection in Deep Geothermal Wells – Application to IDDP-2

Morten Tjelta
Institute for Energy Technology
P.O. Box 40
N-2027 Kjeller
Norway

Bente Cecilie Krogh
Equinor ASA
Arkitekt Ebbels veg 10
7005 Trondheim
Norway

Sturla Sæther
Equinor ASA
Arkitekt Ebbels veg 10
7005 Trondheim
Norway

Marion Seiersten
Institute for Energy Technology
P.O. Box 40
N-2027 Kjeller
Norway

ABSTRACT

In order to make the world's energy consumption sustainable there is a need for reducing emissions of CO_2 and to shift towards renewable energy sources. Geothermal energy has a large potential in certain parts of the world. One example is Iceland, where the reservoir in IDDP-2 is around 427°C and 340 bar at a final well depth of 4650 m. This makes it attractive as a geothermal reservoir of high enthalpy supercritical water with the potential for conversion of large amounts of high temperature deep geothermal energy.

Production from the IDDP-2 is scheduled to start in 2019, and hence the fluid composition is not known. Using available data for nearby wells, and in particular IDDP-1, an estimate can still be made. A combination of high temperature and pressure, the presence of corrosive agents (such as HCl and H_2S), a low pH and reducing conditions gives rise to challenges related to material selections.

This paper summarizes part of a desktop case study that addresses corrosion and scaling issues for conditions relevant for the IDDP-2 geothermal well. The reservoir and well data are based on temperature measurements inside the well and assumptions on a hydrostatic reservoir. The total depth of the well is 4650 meters. Based on this a model is set up for temperature and pressure profile along the well. Knowledge gaps, such as lacking solubility data and corrosion rates at supercritical conditions are pointed out.

Key words: Geothermal energy, deep geothermal energy, DGE, silica, scaling, corrosion

INTRODUCTION

The background for this paper is the desired utilization of deep geothermal energy in general and the IDDP-2 well (Iceland Deep Drilling Project[1]) in special. IDDP is aimed to achieve production of geofluids from a field with supercritical water conditions. An attractive feature of production from a supercritical reservoir is that it potentially can generate a higher power output than conventional high-temperature wells.[2] In theory, it is possible to produce such a field as dry superheated steam, i.e. with no water condensation during normal production. This has desirable features, which will be discussed later.

Several books and reviews have been written on supercritical water (SCW) and geothermal energy. Much of the literature on supercritical water comes from the field of supercritical water reactors and supercritical water oxidation.[3,4] Although a lot of knowledge can be extended from this to deep geothermal wells on Iceland, one should remember that the conditions in the latter are much more reducing and will as such more resemble those in supercritical water gasification.[5] Fundamental properties of supercritical water are described in the book by Brunner.[6] Corrosion in SCW systems have been reviewed by Kritzer [7] and by Nogara and Zarrouk with the focus on the effect of fluids [8] and materials and materials testing.[9] Use of molecular simulations to gain insight into properties which are not easily accessible experimentally have also been reviewed.[10]

The aim of this paper is not to give a conventional review, but rather to give a more practical approach as to how information and correlations available in literature can be applied to, as a first approximation, evaluate the potential for corrosion and scaling in a deep geothermal energy (DGE) system. Knowledge obtained from this will add quality to the on-site experimental campaign during the IDDP-2 test period.

Fundamentals

When water is at conditions above the critical temperature (374°C) and pressure (220.6 bar) it exists as a single supercritical phase. The properties are somewhat between those of a liquid and those of a gas, e.g. having typically a high density and a low viscosity.[11] Above the critical point the hydrogen bonding is minimized.[12] As the density decreases the distance between molecules must necessarily increase and an intramolecular force such as hydrogen bonding becomes weaker. While ambient water is a good polar solvent and effectively dissolves ionic species, supercritical water behaves more like a non-polar solvent and can effectively dissolve gases and organic compounds. For example, supercritical water and oxygen are completely miscible.[11]

Superheated steam is dry at a temperature well above the boiling point, saturated steam is steam at the dew point; i.e. at the boiling point at the given pressure, and supercritical steam is steam above the supercritical point. Non-volatile solutes present in the fluid will increase the stability window of the liquid phase and raise the critical point. The presence of volatile species and gases such as CO_2, HCl and H_2S, however, will lower the critical point. For seawater, the critical temperature will be higher than in pure water, for instance a 3.2 wt% NaCl solution has a critical point at 407 °C and 298.5 bar.[13] Although salts and gases shift the critical point in the opposite direction, the practical situation is usually that the critical point is shifted slightly upwards with respect to pure water.[14] In order to have a complete set of pressure-temperature-density data, this paper will use that of pure water in further evaluations.

Description of tools and relations used in this study

Phase relations and fundamental properties of pure water are available for conditions extending well into the supercritical regime.[6,15] The formulation used in IAPWS-95 is based on Helmholtz energy as a function of temperature and density and can be used to derive any thermodynamic property within its validity range.[16] This range extends up to 1000 °C and 10000 bar, and is therefore applicable to any temperature and pressure one may encounter in geothermal applications.

Dissociation (or ionization) of pure water is described in IAPWS R11-07 [15] which is based on data and analysis by Bandura and Lvov.[17] The relation, which is semi-empirical and takes temperature and water density as inputs, is not repeated here – and the reader is referred to other literature [6,15,17] for a full description. Water ionization is represented well by the relation in question in the temperature range 25 – 800 °C and for densities up to 1.25 g·cm^{-3}.

For HCl dissociation there are several relations available in the literature with different regions of applicability. Typically, they are functions of temperature and water density with the general form

$$\log\left(K_d\right) = A + BT + \frac{C}{T} + D \cdot \log\left[\rho_{\mathrm{H2O}}\left(T\right)\right] + E \cdot \log\left(T\right) \qquad 1$$

where *A*, *B*, *C, D* and *E* are constants taking different values depending of the region from where they were regressed, while ρ_{H2O} is the water density and *T* is the temperature. Constants valid from 400 to 500 °C between 1500 and 2000 bar are given in.[18] Frantz and Marshall [19] presented a relation from experiments between 100 and 700 °C between 400 and 4000 bar. Converted to densities this covers the range from 0.4 to 1 g·cm^{-3}. Yet another relation, which is applicable for steam, can be found in the book by Brunner.[6] In this work we use the values from Frantz and Marshall,[19] which is the relation also used in the review by Kritzer.[7]

Solubility of quartz was studied by Kennedy along the saturation line and also extending up to 1000 bar and 542 °C.[14] The work includes smooth solubility curves, but no equation was formulated, although it was suggested that it could be done. Simple relations valid up to 250 °C, taking only the temperature as an input, for different polymorphs of silica can be found in literature.[20] Fournier and Potter published an equation correlating quartz solubility up to 900 °C and 10000 bar, taking water density (specific volume) and temperature as inputs.[21] It should be noted that the equation can be used in the stated range as long as the density is between 100 and 1000 g·L^{-1}. For less dense fluids, with density between 10 and 100 g·L^{-1}, the valid temperature range is 300 – 600 °C. Nevertheless, it is the most general equation for quartz solubility in pure water and therefore the one used in this work.

Amorphous silica has a much higher solubility than quartz. A simple correlation at the vapor pressure valid up to 250 °C exists.[22] In the same work, an equation valid along the 1034 isobar up to 380 °C was also presented. Another work gives a temperature dependent relation along the line of saturated vapor pressure up to 350 °C.[23] The task of obtaining solubility data for amorphous silica becomes more challenging with increasing temperature, since amorphous silica is a metastable phase and quartz becomes the dominant phase.

On the relatively short residence time in geothermal energy production, it is possible to utilize the difference in solubility and the kinetic limitation to avoid or at least limit silica scaling. For measurements of solubility, however, the timescale is longer to ensure equilibrium, and one run into the risk of precipitating quartz instead of amorphous silica.

Pressure-temperature profile and constant enthalpy production

Whether or not it is possible to produce the fluid in IDDP-2 without entering the two-phase region remains to be seen. All available information thus far indicates that the conditions in the reservoir are indeed supercritical. Between the reservoir and the production pipe there will be some pressure loss (drawdown), which is expected to be some tens of bars. With the relatively warm surroundings of the well, the heat loss is expected to be small. As a first approximation it is assumed that there is no heat loss, and that the loss of pressure during fluid production in the well is due to friction loss and static height. For fluid flow in a straight tube the pressure friction loss, Δp, is given by

$$\Delta p = 4 f \frac{L}{D} \rho \frac{v^2}{2} \qquad 2$$

Where L is the tube length, D is the diameter, ρ is the fluid density, v is the flow velocity and f is a friction coefficient. The friction coefficient is expressed as a function of the Reynolds number (Re), but becomes fairly constant at high Re.[24] An assumption is made that the changes in density and flow velocity will cancel each other out (the density decreases as the fluid expands and the velocity goes up), so that Δp scales linearly with the tube length (i.e. well depth). The resulting temperature and density are then simply what would be required to keep the enthalpy of the fluid constant.

RESULTS

An early estimate of the reservoir in IDDP-2 was around 450°C and 350 bar. Such estimates can be based on a temperature measurement, and simply calculate the corresponding pressure based on a hydrostatic model. Assuming for simplicity that this is pure water, the corresponding enthalpy is 2671 kJ·kg^{-1}. Newer estimates for the reservoir have suggested 435 °C and 300 bar, and bottom hole conditions of 427 °C and 340 bar have been put forward. These sets give somewhat different enthalpy, 2708 and 2450 kJ·kg^{-1} assuming pure water. For the more phenomenological approach taken in this work, set of values 450°C, 350 bar and 2671 kJ·kg^{-1} was chosen, together with a rounded length of 4500 m. The main effect of having a lower temperature and pressure in the well is that the temperature and pressure will be lower top-side (given everything else equal). In order to illustrate this, pressure and temperature profiles are shown in Figure 1 for reservoirs having the same enthalpy but different pressures. Note that these are simplified figures, since in reality the lower pressure fluid would have a lower density and therefore a smaller pressure drop according to Eq. 2 (the curve would have a smaller slope). This would propagate through the temperature and density profiles as well. The approach still serves as a conservative first estimate of the temperature and pressure drop during fluid production.

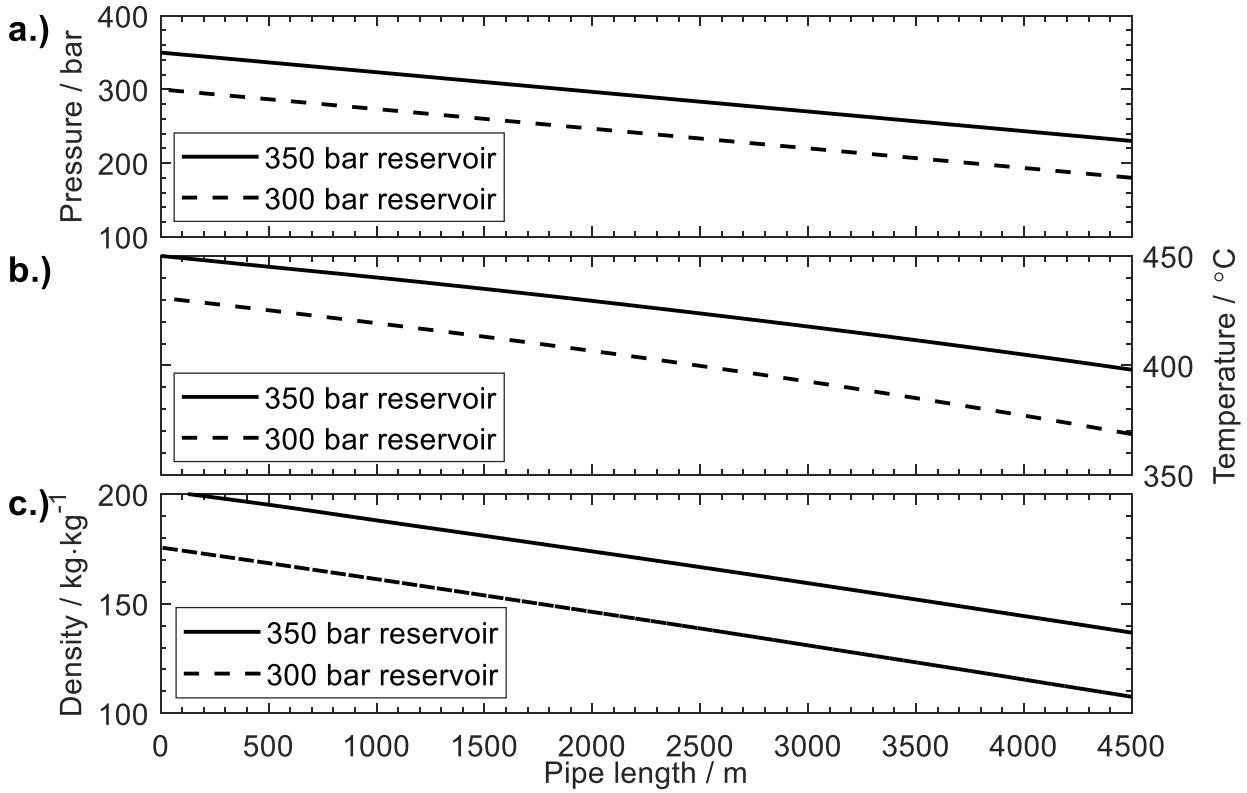

Figure 1: Pressure (a), temperature (b) and density (c) profiles along a 4500 m long pipe. Pressure is assumed a linear function of length only, with Δp = 120 bar across the pipe length.

Figure 2 shows the density for water as a function of temperature for selected pressures. Beyond the supercritical temperature the density is still high, but gradually decreases upon further increasing the temperature. From the figure, the variation in density is largest around the supercritical point.

The black dashed line in Figure 2 follows the line for constant enthalpy during depressurization of our fluid. Note that the lower temperature where pure water with an enthalpy of 2671 kJ·kg^{-1} exists only as a gas is 329°C (and 126.8 bar). Below this, the constant enthalpy line crosses into the two-phase region where liquid water is expected. The point of crossing over into the two-phase region can also be seen in a plot of enthalpy as a function of temperature, which is shown in Figure 3 for selected isobars and along the saturated vapor pressure. For the values considered in this example, it should be possible to produce the fluid as superheated steam, i.e. without going into the two-phase region, if the heat- and friction losses are kept at a minimum. The benefits of avoiding the two-phase region are discussed further in the section on corrosion below. It should be noted that an additional pressure loss between the reservoir and the well is expected. This will bring the fluid closer to the two-phase region in the upper part of the well, but steam production may still be achievable.

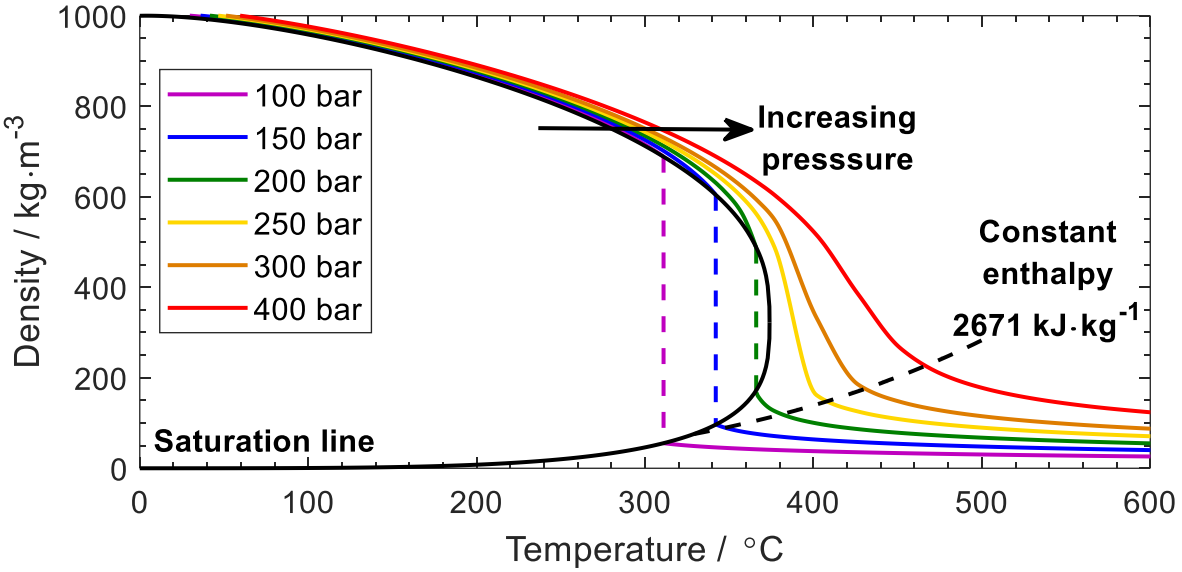

Figure 2: Isobaric density for water as a function of temperature for selected pressures. Also included is the density along the saturation line. Data were obtained from literature.[16] The black dashed line follows a constant enthalpy.

Thermodynamic data is the basis for calculating and predicting phase stability and the possibility for corrosion, scale formation, film formation and precipitation. It is customary to base such calculations on the minimization of Gibbs or Helmholtz energy. They are both strong functions of temperature and given by internal energy, enthalpy and entropy. The three latter show steady variations with temperature below the critical point but are insensitive to changes in pressure here where the fluid is essentially incompressible. Around the critical point there are significant variations, both as a function of temperature and pressure, cf. the enthalpy shown in Figure 3.

To maximize the output of a geothermal system one would like to have a fluid with as high enthalpy as possible. Higher enthalpy would in general imply a higher temperature and therefore a deeper well [25]. This will again increase capital cost and can also introduce new engineering challenges. At higher temperatures, a reservoir with a low pressure will have higher gravimetric enthalpy than a reservoir with a high pressure, cf. Figure 3. A lower pressure will ease the strength requirements for the construction materials involved, which can be expected to lower the capital costs. In this respect, an optimal reservoir will be one of low pressure and high temperature.

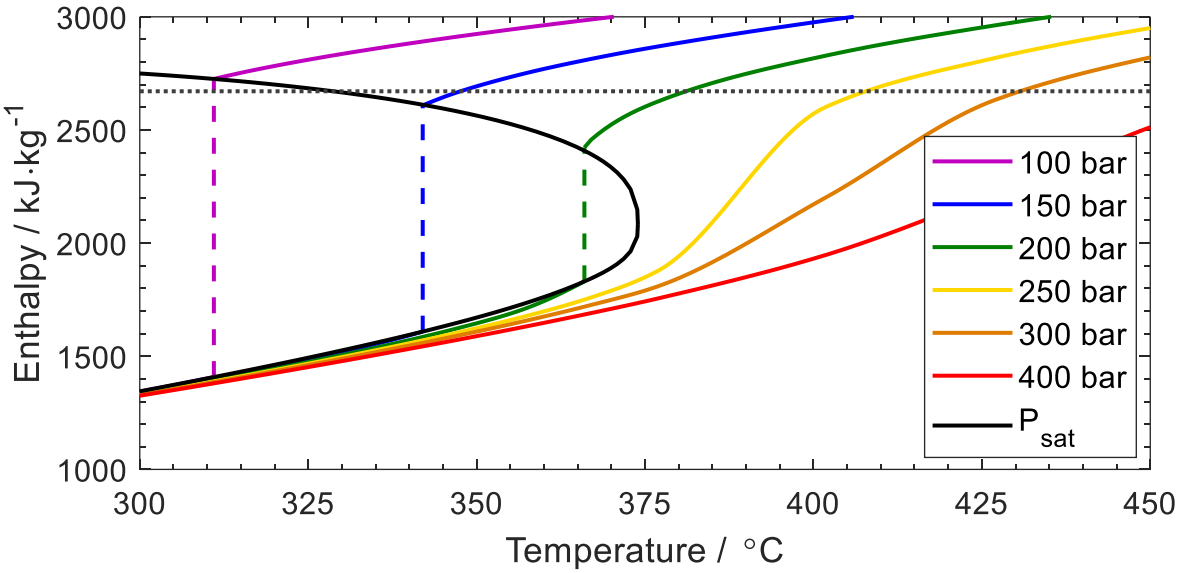

Figure 3: Isobaric enthalpy (*H*) for water as a function of temperature for selected pressures. Also included is the enthalpy along the saturation line. Data were obtained from literature.[16]

Expected conditions in IDDP-2

Armannsson et al.[26] give more detailed analyses of the steam from IDDP-1 and the wells KG-12 and KJ-36 at Iceland, see Table 1. The analyses confirm the reducing conditions with the presence of H_2, but it also shows that the concentrations vary considerably among the different fields at Iceland. The variation in CO_2 and H_2S concentration affects the corrosivity of the fluid. The analyses of the superheated steam do not contain any condensables for IDDP-1, but they are listed in Ref. [26]. The origin of Cl or Cl^- is probably HCl. Presence of HCl corresponds well to the measured pH for IDDP-1. Converted to mol/kg the value corresponds to $2.5 \cdot 10^{-3}$; as H^+ which gives pH ca. 2.6. For the other two wells there seem to be other sources of Cl^- in addition as the pH in the water is higher.

Table 1: Gas composition and selected condensables in samples from IDDP-1, KG-12 and KJ-36 at Iceland.[26] The last column show the composition of superheated steam from IDDP-1 (240-270 °C).[27]

Gas or condensable	IDDP-1 (2012)	KG-12 (1979)	KJ-36 (2007)	IDDP-1 steam
CO_2 (mg/kg)	560	17077	6463	339
H_2S (mg/kg)	250	1127	3320	732
H_2 (mg/kg)	8.77	44.6	32.8	10
N_2 (mg/kg)	16.3	0	175	
CH_4 (mg/kg)	0.27	6.7	2.7	
Ar (mg/kg)	0.53		3.6	
Cl (mg/kg)	90	112	400	93
SiO_2 (mg/kg)	6.2	28		
Na (mg/kg)	0.08	0.17		
K (mg/kg)	0.02			
Ca (mg/kg)	<0.1	0.43		
SO_4 (mg/kg)	5.78		6.5	
Other parameters				
pH	2.4	3.5	3.3	2.7

Fridriksson et al.[28] have estimated the composition of the fluid to be produced in IDDP-2. They expect that the water originates from seawater and may contain 3.5% NaCl. For the production and to estimate the composition of the produced fluids, they consider three scenarios for the bottom-hole temperature (enthalpy) and from that discuss the properties of the produced fluids. The scenarios are 1: 382°C (1830 kJ/kg), 2: 441°C (2470 kJ/kg) and 3: 550°C (3256 kJ/kg). In scenario 1, NaCl will be produced with the fluids, while the NaCl content in the fluid will depend on the phase that is produced in scenario 2 and in scenario 3, it is likely that the NaCl will be left behind.[28]

The silica content in the produced fluid is estimated and there is some discussion of corrosivity and precipitation of salt as follows (adiabatic production assumed).[28] The estimated silica in scenario 1 is around 900 mg/kg. Two-phase field will be reached during production and saturation with respect to amorphous silica will be reached at around 275°C and 60 bar. Metal sulphide scaling is also expected, not because of H_2S, but because of high solubility of sulphides in the reservoir. Scenario 2 has an estimated silica content of 200 mg/kg, and possible separation into two fluids (two liquids: dilute & brine).[29] Production of concentrated brine will be problematic and only production of dilute brine can occur. That will have low salt (NaCl) content but may contain considerable amounts of HCl. If condensation occurs in the well, the water will be very corrosive due to the HCl. For the third scenario with ~200 mg/kg silica, the fluid can be brought to the surface as superheated steam with no liquid condensation. Silica is expected to precipitate as amorphous dust. It is expected that the fluid will have a high HCl concentration, several 100 mg/kg of Cl.

Corrosive species in supercritical water

The density of supercritical water is the most important parameter for corrosion [6] and direct correlations between corrosion rates and the density and ionic product of the fluid have been developed.[30] In a system with large density variations it is beneficial to express concentrations on a molar or mass basis (e.g. molar fraction) rather than on a volumetric basis (e.g. mol/L). Regardless of temperature and pressure a system with a high density (> 200 $kg \cdot m^{-3}$) is capable of dissolving ionic compounds and thereby promote corrosion.[5] This means, in general, that a high pressure high density supercritical fluid is more corrosive than a low pressure low density fluid at the same temperature. Note, however, that the possible formation of protective layers and scales may complicate the picture and make generalizing predictions less straight forward.

The density of the fluid in IDDP-2 is in the region of what would be characterized as a low-density fluid and, hence also a low-corrosivity fluid. This suggests that as long as the fluid is in the supercritical state, or a superheated steam, the corrosivity of the fluid should be manageable. If, however, one crosses into the two-phase region where a liquid phase is formed, the situation changes dramatically.

Dissociation of water into protons and hydroxide is a function of both temperature and pressure, as shown in Figure 4. Three selected isobars and the 2671 $kJ \cdot kg^{-1}$ constant enthalpy are included. The estimated neutral pH (not taking how fugacity/activity coefficients vary with temperature and pressure into account) at 300°C and 250 bar, is 5.6. It means that water can be considered more acidic at high (but sub-critical) conditions, in the respect that the activity of H^+ increases. Also, the OH^- activity increases at these conditions, since during self-dissociation of water the activity of H^+ and OH^- become the same. An example of the effect of this is the fact that near-critical water is a good source of protons in terms of catalyzing acid-catalyzed reactions.[12]

One would then expect corrosion rates to increase with increasing temperature and reach a maximum around 300°C for processes where proton reduction (hydrogen evolution) is the cathodic reaction. At even higher temperatures and going beyond the supercritical temperature one would expect corrosion rates determined by proton reduction to reduce significantly because of the increase in pK_w.

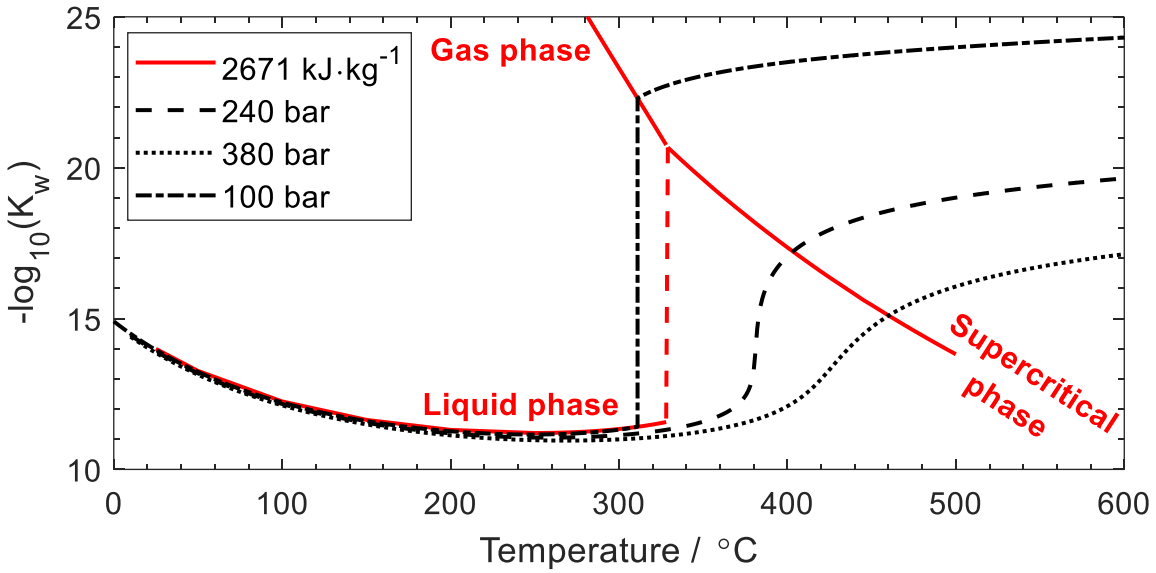

Figure 4: Ionization constant for water as a function of temperature for the 2671 kJ·kg^{-1} constant enthalpy and for selected isobars as indicated in the legend

Increased hydroxide concentrations will increase the saturation ratio of hydroxides and oxy-hydroxides and will therefore increase the tendency for precipitation of such compounds. Hydroxide is involved in certain corrosion mechanisms, for example as an adsorbed intermediate in anodic dissolution of iron.[31] If the rate constant for this reaction is also dependent of the hydroxide concentration at high pressure and high temperature, an increase in pK_w could result in higher corrosion rates.

Supercritical water produced from geothermal wells contains non-condensable gases H_2, N_2, CH_4 and Ar, and CO_2 and H_2S in concentrations ranging from some hundred to several thousand ppm.[26] Other components which are present at significant concentrations and which may affect corrosion are HCl and HF. HCl is volatile and the fraction that condenses with water will decrease with increasing temperature

It should also be noted that the fluid contains appreciable amounts of silicon oxide/hydroxide(s) and cations originating from (hydr)oxides or salts. For corrosion it is important whether the conditions are oxidizing or reducing. In oxidizing conditions trans-passive dissolution may be a problem, while under reducing conditions protective oxides may not form. An example of a material that may experience trans-passive dissolution is chromium. At oxidizing conditions, soluble species of hexavalent chromium are thermodynamically stable.

Hydrogen present in the fluid, possibly formed during proton reduction as part of corrosion, or other hydrogen containing compounds may lead to the formation of hydrides. Hydrochloric acid or other chloric containing compounds may lead to the formation of oxy-chlorides or hydroxyl-chlorides which may affect the corrosion mechanism and corrosion rate.

The corrosivity of the minor constituents is highly dependent on the water state. As an example, HCl is a fully dissociated strong acid in liquid water at low temperature. As such, it is highly corrosive when its concentration exceeds, say, 10^{-4} M and it gives a pH below 4. The dissociation constant decreases with temperature and HCl becomes a much weaker acid with hardly any dissociation in supercritical water as shown along selected isobars in Figure 5.

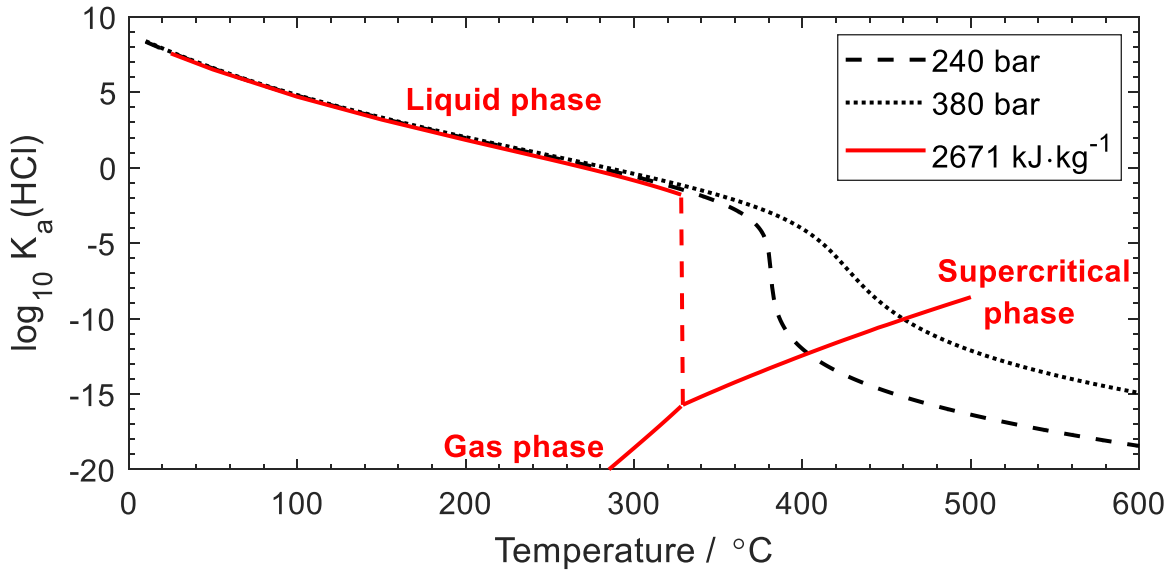

Figure 5: Ionization constant for HCl as a function of temperature for the 2671 kJ·kg^{-1} constant enthalpy and for selected isobars as indicated in the legend

With increasing temperature reaction rate constants increase while the concentration of a corrosive specie such as H^+ decreases going beyond approximately 300 °C as described above. This leads to a maximum in the corrosion rate due to proton reduction (keeping film and scale formation out of the discussion for now) close to the supercritical point. At high supercritical temperatures, undissociated HCl become the major corroding specie. Undissociated HCl is known to be less aggressive than dissociated (i.e. protons), but while the corrosion rate caused by protons has a maximum near supercritical temperature the corrosion rate caused by HCl alone increases with increasing temperature, at least up to 550°C.[30]

Looking at the solid line following constant enthalpy in Figure 5, i.e. the line assumed for IDDP-2, we see that HCl behaves as a weak acid as long as the two-phase region is avoided. Going below 329 °C, however, a liquid phase will form, and this phase will be acidic as the dissociation constant is high and increases with decreasing temperature. One should remember that where HCl acts as a weak acid, the presence of salts such as NaCl will affect dissociation according to equilibrium chemistry. Cl^- is the conjugated base of HCl, meaning that addition of Cl^- will make the system less acidic by shifting the dissociation reaction towards undissociated HCl according to Le Châtelier's principle.

Materials to be evaluated for deep geothermal wells

In addition to temperature and strength requirements, the main parameters that govern the material selection in deep geothermal wells, are the fluid density, minor constituents as HCl and H_2S and the oxygen fugacity. The actual alloys depend on forming a dense oxide film with low permeability of the corrosive species in the fluid. If the fluid contain hydrogen, the oxygen fugacity will be determined by the water formation constant and the water to hydrogen fugacity ratio. When selecting materials, the oxygen fugacity must be seen in connection with the stability of the oxides that constitute the protective films. As a first approximation stability of the common oxides is as follows:

$$Al_2O_3>SiO_2>TiO_2>Cr_2O_3>NiO>Fe_3O_4$$

It is only a coarse guideline, the stability of mixed oxides, hydroxides, other oxidation states and hydrides must also be taken into account.

There is substantial experience with the production of water and steam, even superheated steam, from geothermal wells.[8,32] So far, none has produced supercritical water with high density. When high density supercritical water is used in other applications, it usually contains some oxygen and, hence, is not reducing with respect to any of the oxides listed above.[7,33]

With few exceptions, alloyed steels for use at high temperature contains chromium, and a chromia or mixed iron-chromium layer at the surface determines their corrosion rate. It is not sufficient in high temperature water (>300 °C) if the water contains HCl and H_2S [25,34] or significant amounts of hydrogen.[35] The chromia film on UNS S31600 and N08810 failed even in superheated steam with hydrogen at 600 °C.[36,37] In some tests, it is found that highly alloyed steels as UNS S31254 and N08028 are prone to SCC in water at 330 to 350 °C, but it may be related to thermal stresses experienced during frequent heating and cooling.[34]

Alumina forming austenitic stainless steels have been developed recently.[38] They are primarily developed for aggressive oxidizing environments at 600-900°C. However, as alumina is thermodynamically more stable than chromia at high water activity and reducing conditions, it is worthwhile to consider these as alternatives to chromia formers for geothermal applications with supercritical steam. The steels are reported to perform well compared to chromia-forming alloys in water vapor and steam.[39]

The testing and use of nickel-based alloys in relevant SCW and geothermal application is mostly limited to UNS N06625. Its corrosion resistance depends on forming a chromia rich film at the surface, but in supercritical water the film may contain considerable amounts of nickel. It has shown good performance in geothermal conditions up to 350 °C [34,40] and even in 25 MPa steam with some hydrogen and HCl it was unattacked up to 550 °C.[35]

Titanium alloys have not been extensively tested at relevant geothermal conditions with high density supercritical water. In an early study R56404 and R56320 with Ru was tested regarding use as tubulars and components for corrosive, high temperature geothermal well fluids with H_2S. They were found to be resistant up to 330°C.[41] In a later study at geothermal conditions and temperature up to 350 °C, R52400 showed excellent performance; no cracks or corrosion attacks, while R50400 developed some small cracks.[34]

When one looks at the costs of some of the materials that are candidates for use in deep geothermal wells it becomes apparent that the material selection will be cost driven. However, considerably more knowledge is required to specify the most cost-effective material that is fit for purpose for production of high density supercritical water. This will be part of the future work.

Supercritical water scaling

Geofluids (fluid extracted from geothermal resources) may have many chemical constituents. A figure, covering all types of geofluids, was included Finster et al.[42] The supercritical sources are on that relative scale in the high end on SiO_2, medium to high on chloride and in the lower end on other ions. With a few exceptions silica (SiO_2) and calcium carbonate ($CaCO_3$) are the main chemical compounds that are responsible for scaling in high temperature geothermal operations.[43] Of these silica is the most common and the one expected to pose the largest threat to IDDP-2.

It is widely recognized in literature that the solubility of amorphous silica is much higher than that of quartz and that the kinetics for precipitation of amorphous silica is much faster than that for quartz. This seems, however, to be based on information from systems at somewhat lower temperatures than the ones relevant for IDDP-2.

Figure 6 shows the solubility of quartz and amorphous silica along the saturated vapor pressure (solid lines) and at the 1034 bar isobar. Data for quartz were obtained using data from the NIST database as inputs into the framework in Fournier and Potter.[21] The curves for amorphous silica were obtained using equations from Fournier and Rowe [22] and Gunnarsson [23] at 1034 bar and along the saturation line, respectively. Unfortunately, information on the solubility of amorphous silica at higher temperature is difficult to come by. It can, however, be observed from the figure that the ratio of quartz to amorphous silica solubility increases with temperature. Giving some numerical examples we find that the solubility of amorphous silica is 16 times higher than that of quartz at 25 °C, while around 350 °C it is roughly 2 times larger. The quartz:amorphous solubility ratio is included in the figure as green lines.

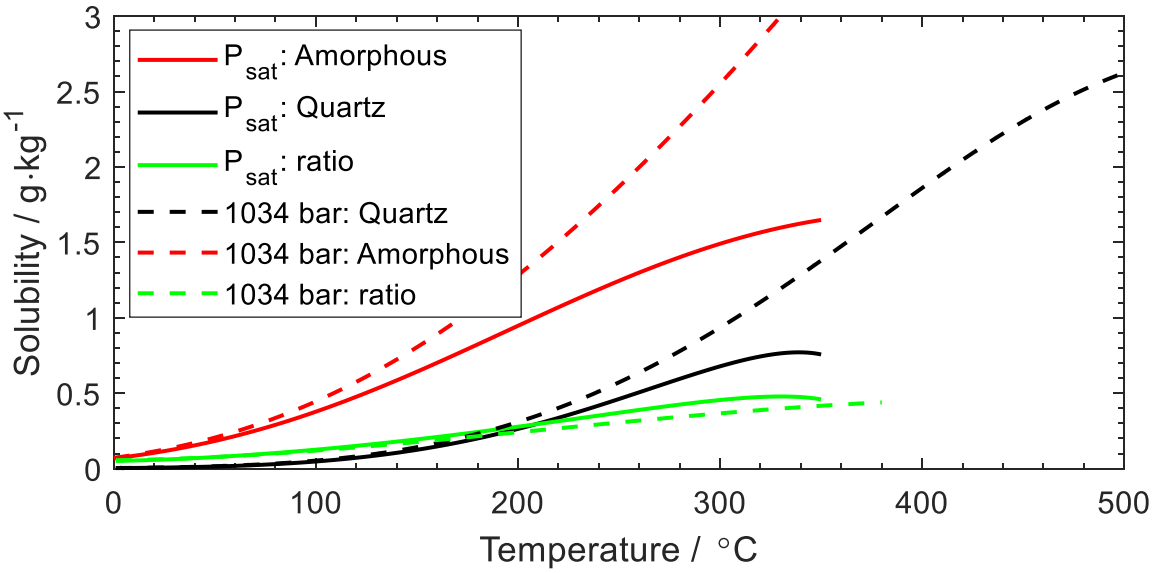

Figure 6: Solubility of quartz and amorphous silica along the vapor pressure of water (solid black and red lines). Dashed lines show the solubility of quartz (black) and amorphous silica (red) at the 1034 bar isobar. Also, are the ratio of quartz to amorphous silica solubility along the saturation line (solid green curve) and along the 1034 bar isobar (green dashed line).

The solubility of quartz along the temperature-pressure profile corresponding to a constant enthalpy of 2671 kJ·kg^{-1} is shown in Figure 7 as the black dashed curve. Also included in the figures, as solid lines for consistency wrt. Figure 6, are the solubilities of quartz and amorphous silica along the saturation line. In the absence of information at higher temperature for amorphous silica, we assume that the ratio at the temperature of maximum quartz solubility (339 °C, ratio = 0.475) can be extended into the supercritical region. Doing this exercise gives the red dotted curve included in the figure. The same simple assumption is used to roughly estimate the amorphous solubility along the 2671 kJ·kg^{-1} isenthalpic line, which is shown as the red dashed line.

The difficulty of obtaining solubility data for amorphous silica at high temperature have been attributed to precipitation of quartz becoming more favorable.[23] This suggests that the kinetics of quartz is sufficiently rapid for it to play a role here. Kinetics of quartz dissolution (and precipitation) have been studied and a relation extending up to 625 °C have been published.[44] An Arrhenius type behavior with temperature was found, and it increases by around 10 orders of magnitude going from 25 to 625 °C. Along the temperature profile from 450 to 329 °C (i.e. from a typical DGE well temperature up to the two-phase region) the rate of quartz precipitation drops by roughly a factor 50.

Scaling can pose a significant threat based on data from binary systems of silica and pure water. The experience from geothermal wells with lower temperature, that the difference in solubility and precipitation kinetics of quartz and amorphous silica can be utilized to avoid scaling, should not be

adopted without further justification. On the other hand, it may be possible to use data from the much more studied quartz system to make some estimates.

Based on the difference in solubility along the constant enthalpy profile, the potential for scaling is around 0.26 g quartz per kg fluid (0.25 $g \cdot kg^{-1}$ if the amorphous phase is assumed to dominate at the estimated solubility). Although this may seem like a small number, with mass flow rates during production in the order of 50 – 100 $kg \cdot s^{-1}$, this sums up to several hundred thousand tons per year.

Due to kinetic limitations, however, the full potential is not expected to precipitate. A detailed evaluation of scaling kinetics is a possible topic for further work, but a simplified calculation suggests that of the order of 0.01 $g \cdot kg^{-1}$ quartz will precipitate during production up to the two-phase region. Here it was assumed that the active surface area was the inside of a smooth 220 mm ID tube and a uniform mass flow rate of 75 $kg \cdot s^{-1}$. The amount of precipitation will depend on the flow rate. With a very high flow rate, the rate of precipitation will be too slow, and scaling will not occur. If the flow rate is low enough, equilibrium will be achieved and all 0.26 $g \cdot kg^{-1}$ will precipitate. Another consequence of a high flow rate not considered in this work, is the resulting sheer forces exerted on the pipe walls.

It should be emphasized that the numbers used in approximations thus far are those for pure water and silica. In a more complex system both thermodynamics and kinetics will change. The solubility of silica increases with increasing pH by enhancing dissociation of silicic acid. Dissolutions rates for quartz are generally found to be independent of pH in the lower end, say below pH 4, and then increase with increasing pH. By decreasing pH from approximately 7 to 4, the dissolution rate of quartz decreased one order of magnitude at 25 °C [45]. The presence of aluminum in the fluid affects precipitation kinetics in the intermediate pH range (5 < pH < 9).[46]

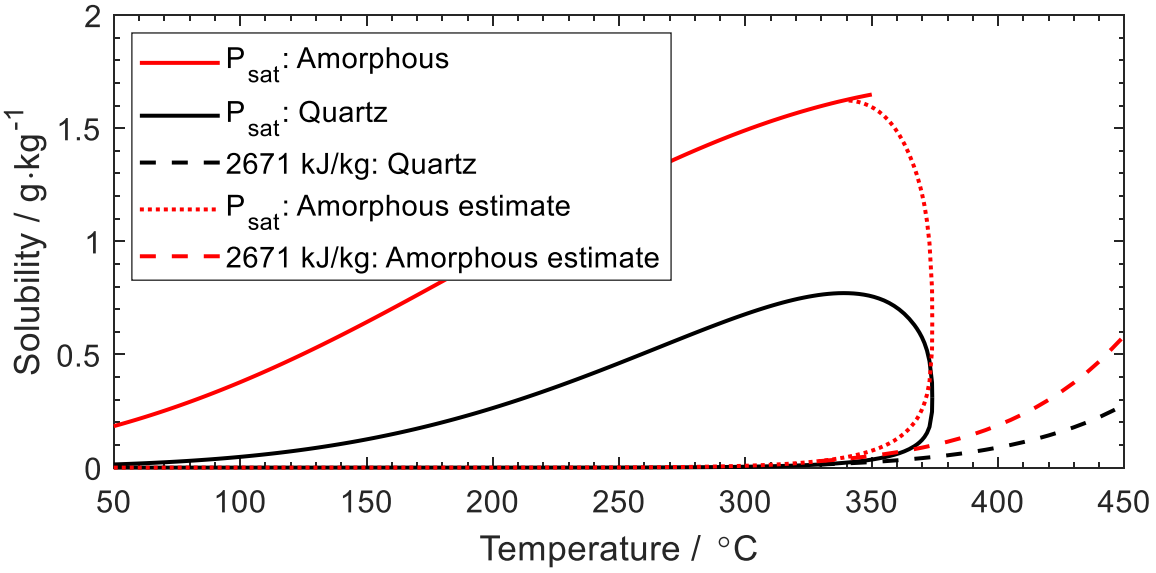

Figure 7: Solubility of quartz (black) and amorphous silica (red) along the saturation line. The red dotted line is an estimate of the solubility of amorphous silica outside the region reported in literature (see text for details). Black dashed line is the calculated solubility of quartz along the temperature-pressure profile corresponding to a constant enthalpy of 2671 $kJ \cdot kg^{-1}$. An estimate of the solubility of amorphous silica along the same profile is shown as the red dashed line.

CONCLUSIONS

Relations found in open literature have been used along the estimated temperature-pressure profile to evaluate corrosivity and scaling potential in a geothermal well where supercritical water flows in to the well. If production of a one-phase fluid is possible, the corrosion issues should be kept at a minimum. In the event of liquid phase formation, this phase is expected to be very corrosive and pose a significant challenge. Note also that even if the fluid could be produced as superheated steam during normal operation, water may drop-out during shut-downs, start-up and irregular production.

At the high temperatures encountered in DGE, both quartz and amorphous silica scaling are possible. An upside of this is that estimates could be based on quartz, for which much more literature data are available. Even though the fraction of precipitation is low, in the order of 10 ppmw, the total amount will be very large due to the high flow rates and measures to limit or control precipitation should be taken. A possible strategy is to investigate further if there is an optimal pH where the solubility is sufficiently high while the precipitation rate is sufficiently low. With IDDP-2 being a quite acidic field, an adjusted pH is expected to be a higher one. This could also prove beneficial when it comes to corrosion.

A more detailed evaluation of IDDP-2 well benefit from a measured composition based on the produced fluid. Also, more data from laboratory tests involving multiple components would be desirable. For the case of IDDP-2 it is expected that the system H_2O-NaCl-SiO_2-HCl would be with the possible inclusion of H_2S should cover the most important aspects.

ACKNOWLEDGEMENTS

This study was financed through the HoTCaSe project, supported by the Research Council of Norway (contract no. 269399). The IDDP-2 was funded by HS Orka, Landsvirkjun, Orkuveita Reykjavíkur, and the National Energy Authority in Iceland, together with Equinor ASA. The IDDP has also received funding from the EU H2020 (DEEPEGS, grant no. 690771).

REFERENCES

1. About IDDP. Retrieved from https://iddp.is/about, 2016.
2. G.Ó. Friðleifsson, W.A. Elders, R.A. Zierenberg, A. Stefánsson, A.P.G. Fowler, T.B. Weisenberger, B.S. Harðarson, K.G. Mesfin, The Iceland Deep Drilling Project 4.5 km deep well, IDDP-2, in the seawater-recharged Reykjanes geothermal field in SW Iceland has successfully reached its supercritical target, Sci. Dril., 23 (2017) 1-12.
3. C. Sun, R. Hui, W. Qu, S. Yick, Progress in corrosion resistant materials for supercritical water reactors, Corrosion Science, 51 (2009) 2508-2523.
4. S. Zhang, Z. Zhang, R. Zhao, J. Gu, J. Liu, B. Örmeci, J. Zhang, A Review of Challenges and Recent Progress in Supercritical Water Oxidation of Wastewater, Chemical Engineering Communications, 204 (2017) 265-282.
5. P.A. Marrone, G.T. Hong, Corrosion control methods in supercritical water oxidation and gasification processes, The Journal of Supercritical Fluids, 51 (2009) 83-103.
6. G. Brunner, Hydrothermal and Supercritical Water Processes, Elsevier Science, Burlington, 2014.
7. P. Kritzer, Corrosion in high-temperature and supercritical water and aqueous solutions: a review, The Journal of Supercritical Fluids, 29 (2004) 1-29.
8. J. Nogara, S.J. Zarrouk, Corrosion in geothermal environment: Part 1: Fluids and their impact, Renewable and Sustainable Energy Reviews, 82 (2018) 1333-1346.
9. J. Nogara, S.J. Zarrouk, Corrosion in geothermal environment Part 2: Metals and alloys, Renewable and Sustainable Energy Reviews, 82 (2018) 1347-1363.

10. J.M. Stubbs, Molecular simulations of supercritical fluid systems, The Journal of Supercritical Fluids, 108 (2016) 104-122.
11. Z.Y. Ding, M.A. Frisch, L. Li, E.F. Gloyna, Catalytic Oxidation in Supercritical Water, Industrial & Engineering Chemistry Research, 35 (1996) 3257-3279.
12. K. Tomita, Y. Oshima, Enhancement of the Catalytic Activity by an Ion Product of Sub- and Supercritical Water in the Catalytic Hydration of Propylene with Metal Oxide, Industrial & Engineering Chemistry Research, 43 (2004) 2345-2348.
13. J.L. Bischoff, R.J. Rosenbauer, Liquid-vapor relations in the critical region of the system NaCl-H2O from 380 to 415°C: A refined determination of the critical point and two-phase boundary of seawater, Geochimica et Cosmochimica Acta, 52 (1988) 2121-2126.
14. G.C. Kennedy, A portion of the system silica-water, Economic Geology, 45 (1950) 629-653.
15. J.P. Cooper, D. R.B., Release on the ionization constant of H2O (R11-07), The International Association for the Properties of Water and Steam (IAPWS), (2008).
16. W. Wagner, A. Pruß, The IAPWS Formulation 1995 for the Thermodynamic Properties of Ordinary Water Substance for General and Scientific Use, Journal of Physical and Chemical Reference Data, 31 (2002) 387-535.
17. A.V. Bandura, S.N. Lvov, The Ionization Constant of Water over Wide Ranges of Temperature and Density, Journal of Physical and Chemical Reference Data, 35 (2006) 15-30.
18. B.R. Tagirov, A.V. Zotov, N.N. Akinfiev, Experimental study of dissociation of HCl from 350 to 500°C and from 500 to 2500 bars: Thermodynamic properties of HCl°(aq), Geochimica et Cosmochimica Acta, 61 (1997) 4267-4280.
19. J.D. Frantz, W.L. Marshall, Electrical conductances and ionization constants of salts, acids, and bases in supercritical aqueous fluids; I, Hydrochloric acid from 100 degrees to 700 degrees C and at pressures to 4000 bars, American Journal of Science, 284 (1984) 651-667.
20. R.O. Fournier, Fournier, R.O. (1989) The solubility of silica in hydrothermal solutions: Practical applications. In: Lectures on geochemical interpretation of hydrothermal water; UNU Geothermal Training Programme, Report 10, Raykjavik, Iceland, 1989.
21. R.O. Fournier, R.W. Potter, An equation correlating the solubility of quartz in water from 25° to 900°C at pressures up to 10,000 bars, Geochimica et Cosmochimica Acta, 46 (1982) 1969-1973.
22. R.O. Fournier, J.J. Rowe, Solubility of amorphous silica in water at high-temperatures and high-pressures, American Mineralogist, 62 (1977) 1052-1056.
23. I. Gunnarsson, S. Arnórsson, Amorphous silica solubility and the thermodynamic properties of H4SiO°4 in the range of 0° to 350°C at Psat, Geochimica et Cosmochimica Acta, 64 (2000) 2295-2307.
24. S. Skogestad, Prosessteknikk: Masse- og Energibalanse, Tapir, Trondheim, 2000.
25. S.N. Karlsdóttir, T. Jonsson, A. Stefánsson, Corrosion Behavior of High Alloy Austenitic Stainless Steel in Simulated High Temperature Geothermal Environment, Corrosion/2017, (2017), paper no. 9280, NACE International, Houston
26. H. Armannsson, T. Fridriksson, G.H. Gudfinnsson, M. Olafsson, F. Oskarsson, D. Thorbjornsson, IDDP-The chemistry of the IDDP-01 well fluids in relation to the geochemistry of the Krafla geothermal system, Geothermics, 49 (2014) 66-75.
27. I.O. Thorbjørnsson, S.N. Karlsdottir, A. Einarsson, K.R. Ragnarsdottir, Materials for Geothermal Steam Utilization at Higher Temperatures and Pressure, in: World Geothermal Congress 2015, Melbourne, Australia, 2015.
28. T. Fridriksson, A. Stefánsson, F. Óskarsson, E. Eyjólfsdótti, O. Sigurdsson, Fluid Chemistry Scenarios Anticipated for IDDP-2 to be Drilled in Reykjanes, Iceland, in: World Geothermal Congress 2015, Melbourne, Australia, 2015.
29. T. Driesner, C.A. Heinrich, The system H2O–NaCl. Part I: Correlation formulae for phase relations in temperature–pressure–composition space from 0 to 1000°C, 0 to 5000bar, and 0 to 1 XNaCl, Geochimica et Cosmochimica Acta, 71 (2007) 4880-4901.
30. L.B. Kriksunov, D.D. Macdonald, Corrosion in Supercritical Water Oxidation Systems: A Phenomenological Analysis, Journal of The Electrochemical Society, 142 (1995) 4069-4073.

31. A. Dugstad, Fundamental Aspects of CO2 Metal Loss Corrosion - Part 1: Mechanism, Corrosion/2003, (2003), paper no. **6111**, NACE International, Houston
32. K. Lichti, Materials Selection Challenges for Geothermal Energy Projects, (2017), paper no. Paper No. 2017-9258, NACE International, Houston, TX, NACE
33. S. Sarrade, D. Féron, F. Rouillard, S. Perrin, R. Robin, J.-C. Ruiz, H.-A. Turc, Overview on corrosion in supercritical fluids, The Journal of Supercritical Fluids, 120 (2017) 335-344.
34. S.N. Karlsdottir, I.O. Thorbjornsson, K.R. Ragnarsdottir, A. Einarsson, Corrosion Testing of Heat Exchanger Tubes in Steam from the IDDP-1 Exploratory Geothermal Well in Krafla, Iceland, (2014), paper no. Paper No. 2014-4152, NACE International, Houston TX, NACE
35. R. Fujisawa, K. Nishimura, T. Nishida, M. Sakaihara, Y. Kurata, Y. Watanabe, Corrosion Behavior of Ni Base Alloys and 316 Stainless Steel in Less Oxidizing or Reducing SCW Containing HCl, (2005), paper no. Papepr No. 05392, NACE International, Houston TX, NACE
36. K.I. Choudhry, R.A. Carvajal-Ortiz, D.T. Kallikragas, I.M. Svishchev, Hydrogen evolution rate during the corrosion of stainless steel in supercritical water, Corrosion Science, 83 (2014) 226-233.
37. K.I. Choudhry, D.A. Guzonas, D.T. Kallikragas, I.M. Svishchev, On-line monitoring of oxide formation and dissolution on alloy 800H in supercritical water, Corrosion Science, 111 (2016) 574-582.
38. M.P. Brady, Y. Yamamoto, M.L. Santella, P.J. Maziasz, B.A. Pint, C.T. Liu, Z.P. Lu, H. Bei, The development of alumina-forming austenitic stainless steels for high-temperature structural use, Jom, 60 (2008) 12-18.
39. K.R. Larsen, Alumina-Forming Austenitic Alloys Resist High-Temperature Corrosion, Mater. Perform., 54 (2015) 30-34.
40. S.N. Karlsdottir, I.O. Thorbjornsson, Corrosion Testing Down-Hole in Sour High Temperature Geothermal Well in Iceland, (2013), paper no. Paper No. 2013-2550, NACE International, Houston TX, NACE
41. R.W. Schutz, Performance Of Ruthenium-Enhanced Alpha-Beta Titanium Alloys In Aggressive Sour Gas And Geothermal Well Produced-Fluid Brines, (1997), paper no. Paper No. 97032, NACE International, Houston, TX, NACE
42. M. Finster, C. Clark, J. Schroeder, L. Martino, Geothermal produced fluids: Characteristics, treatment technologies, and management options, Renewable and Sustainable Energy Reviews, 50 (2015) 952-966.
43. K.L. Brown, Thermodynamics and kinetics of silica scaling, Proceedings International Workshop on Mineral Scaling 2011, (2011), paper no.,
44. J.W. Tester, W.G. Worley, B.A. Robinson, C.O. Grigsby, J.L. Feerer, Correlating quartz dissolution kinetics in pure water from 25 to 625°C, Geochimica et Cosmochimica Acta, 58 (1994) 2407-2420.
45. W. Gabriel Worley, Dissolution kinetics and mechanisms in quartz- and grainite-water systems, PhD thesis, MIT, 1994.
46. D.L. Gallup, Aluminum silicate scale formation and inhibition: Scale characterization and laboratory experiments, Geothermics, 26 (1997) 483-499.